JME

Journal of Mining & Environment,
Vol.4, No.2, 2013, 133-146.

Approximate resistivity and susceptibility mapping from airborne electromagnetic and magnetic data, a case study for a geologically plausible porphyry copper unit in Iran

M. Abedi[1*], G. H. Norouzi[1], N. Fathianpour[2], A. Gholami[3]

1. Department of Mining Engineering, College of Engineering, University of Tehran, Iran
2. Department of Mining Engineering, Isfahan University of Technology, Iran
3. Institute of Geophysics, University of Tehran, Iran

Received 7 April 2012; received in revised form 13 January 2013; accepted 23 January 2013
**Corresponding author: maysamabedi@ut.ac.ir (M. Abedi).*

Abstract
This paper describes the application of approximate methods to invert airborne magnetic data as well as helicopter-borne frequency domain electromagnetic data in order to retrieve a joint model of magnetic susceptibility and electrical resistivity. The study area located in Semnan province of Iran consists of an arc-shaped porphyry andesite covered by sedimentary units which may have potential of mineral occurrences, especially porphyry copper. Based on previous studies, which assume a homogenous half-space earth model, two approximate methods involving the Siemon and the Mundry approaches are used in this study to generate a resistivity-depth image of underground geologically plausible porphyry unit derived from airborne electromagnetic data. The 3D visualization of the 1D inverted resistivity models along all flight lines provides a resistive geological unit which corresponds to the desired porphyry andesite. To reduce uncertainty arising from single geophysical model, i.e., the resistivity model acquired from the frequency domain electromagnetic data, a fast implementable approach for 3D inversion of magnetic data called the Lanczos bidiagonalization method is also applied to the large scale airborne magnetic data in order to construct a 3D distribution model of magnetic susceptibility, by which the obtained model consequently confirms the extension of an arc-shaped porphyry andesite at depth. The susceptible-resistive porphyry andesite model provided by integrated geophysical data indicates a thicker structure than what is shown on the geological map while extends down at depth. As a result, considering simultaneous interpretation of airborne magnetic and frequency domain electromagnetic data certainly yield lower uncertainty in the modeling of andesite unit as a potential source of copper occurrences.

Keywords: *Electromagnetic and Magnetic data, Approximate inversion, Electrical resistivity, Magnetic susceptibility, Porphyry copper unit.*

1. Introduction

Electromagnetic (EM) methods are advantageous to investigate the electrical resistivity variation for anomaly mapping in variety of fields especially mineral/oil and water exploration. The calculation of apparent electrical resistivity is accustomed as the first step of evaluating frequency domain electromagnetic (FEM) data. The lateral resistivity distribution of an area under the FEM prospect can be displayed by apparent resistivity maps at single frequencies. The vertical resistivity distribution is also explored by analysing the EM fields belonging to all surveyed frequencies. The results can be displayed as sounding curves, if depth information

is available, or as resistivity-depth cross-sections [1].

Many mathematical techniques have been developed to interpret the helicopter borne electromagnetic (HEM) data in order to acquire depth images that present resistivity distribution along geological sections. All of which fall into two categories comprising of (1) the direct transformation of observed EM data based on a model of half-space (e.g. [1-10]), and (2) the inversion of EM data assuming a multi-layered earth model by iterative methods to satisfy a multi-constraint objective cost function in optimization problem (e.g. [11-22]).

In this study we work on both airborne FEM data along with magnetic data conducted over the Kalat-e-Reshm area near Semnan province of Iran. The main focus is on the interpretation of the resistivity models from 1D direct inversion of the FEM data by two straightforward methods consisting of the Mundry and the Siemon approaches which have been previously developed and applied in many researches, and also airborne magnetic data to generate a magnetic susceptibility model. Handling airborne data for the sake of large dataset is a problem when an inverse method is applied. Therefore, we have applied a novel method (i.e., the Lanczos bidiagonalization) for the inversion of large scale magnetic data which has been previously published by authors in the case of ground based magnetic prospect. Running time of airborne magnetic data inverse modeling significantly decreases by using the Lanczos method [23]. Joint interpretation of FEM and magnetic data reduces the uncertainty arising from modeling of a single geophysical dataset to image a desired geological unit. To reduce such ambiguous interpretation, integrated geophysical data are currently underway. Using simultaneous interpretation of airborne magnetic and FEM data certainly yields lower uncertainty in geophysical exploration.

The main focus of previous studies in this area was on the FEM data that proved existence of an arc-shaped porphyry andesite having high resistivity property. This resistive geological structure was also confirmed by ground-based electrical resistivity data. The previously processed airborne magnetic data in the Kalat-e-Reshm area were in well agreement with the real location of the andesite unit [24-26]. Since magnetic susceptibility model can play an important role in mineral exploration especially in the cases of investigating porphyry type deposits, we have constructed the 3D distribution of magnetic susceptibility in the desired area to compare it with the resistivity structure. The obtained results show that the joint models of magnetic susceptibility and electrical resistivity are in good agreement with the arc-shaped andesite in the study area, and both models confirm that the structure goes down at depth. Another point which should be noted is that of high resolution images derived from airborne FEM data at surface or shall depths. The FEM data are not proper for detecting extension of geological structures at greater depths. So, retrieving a model of magnetic susceptibility simultaneously can be impressive in this case study to interpret a plausible porphyry unit in mineral occurrences exploration. The resolution of magnetic data to image deeper structures is higher than airborne FEM data.

2. Methodology

Among various types of airborne EM methods, HEM is the one in which the transmitting and measuring system (bird) is towed at a sufficiently large distance below the helicopter and is kept at about 30–40 m above prospected ground surface. This configuration is capable enough to survey and acquire high quality data within a short time for a vast region of interest [10]. Commonly, several geophysical methods are used simultaneously in an airborne survey. A typical helicopter-borne geophysical system operated by the German Federal Institute for Geosciences and Natural Resources (BGR) is shown in Figure 1. It includes geophysical sensors that collect five-frequency electromagnetic, magnetic, and gamma-ray spectrometry data, as well as altimeters and positioning systems [27, 28].

In what follows, we describe the forward formulation of a multi-layered earth model when a horizontal coplanar (HC) configuration in the HEM survey is used. The formulation of approximate direct inversion of such EM data is also explained concisely to be applied on synthetic and real FEM data.

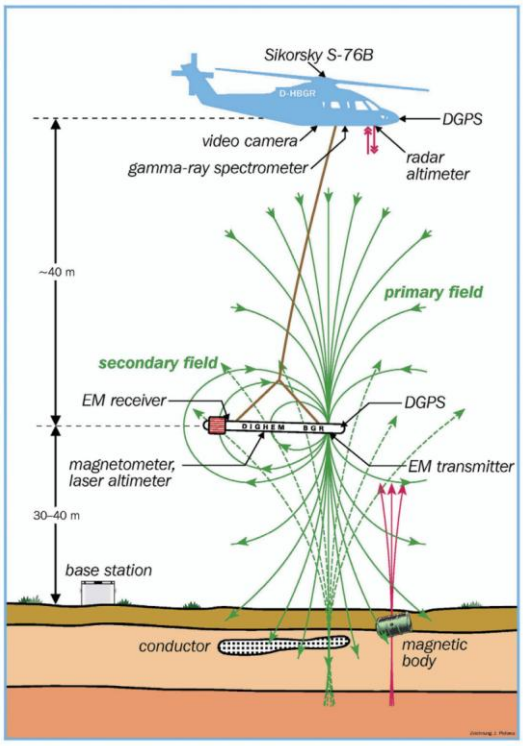

Figure 1. BGR's helicopter-borne geophysical data acquisition system: Electromagnetic, magnetic, GPS and laser altimeter sensors are housed by a "bird", a cigar-shaped 9 m long tube, which is kept at about 30–40 m above prospected ground surface. The gamma-ray spectrometer, additional altimeters and the navigation system are also installed into the helicopter [27, 28].

2.1. 1D EM forward modeling

The EM response of a layered half-space (Figure 2a) for dipole source excitation is given by [29-31], among others. If a HC system is at a height *h* above the layered half-space, the secondary magnetic field H_s, normalized against the primary field H_0 at the receiving coil, is

$$\frac{H_S}{H_0} = R + iQ = s^3 \int_0^\infty R(\lambda)\lambda^2 \exp\left(-2u_0 h\right) J_0(\lambda s)\, d\lambda \qquad (1)$$

where *R*, *Q* are in-phase (real) and out-of-phase (quadrature) components, *i* is the imaginary number, *s* is the coil separation, λ is the variable of integration, and J_0 the Bessel function of the first kind of order zero. The term $R(\lambda)$ can be written as

$$R(\lambda) = \frac{Y_1 - Y_0}{Y_1 + Y_0} \qquad (2)$$

where $Y_0 = u_0 / i\omega\mu_0$ is the intrinsic admittance of free space, Y_1 is the surface admittance, ω is the angular frequency, μ_0 is the magnetic permeability of free space, and u_0 is equal to $\left(\lambda^2 + k_0^2\right)^{1/2}$, where k_0 is the wave number of free space. For a L-layer earth, Y_1 can be obtained by the following recurrence relation,

$$Y_l = \hat{Y}_l \frac{Y_{l+1} + \hat{Y}_l \tanh(u_l t_l)}{\hat{Y}_l + Y_{l+1} \tanh(u_l t_l)}, \quad l = 1, 2, \ldots, L-1, \qquad (3)$$

Where

$$\hat{Y}_l = \frac{u_l}{i\omega\mu_0\mu_l} \qquad (4)$$

and

$$u_l = \left(\lambda^2 + k_l^2\right)^{1/2} \qquad (5)$$

where k_l is the wave number of l th layer given by

$$k_l = \left(i\omega\sigma_l\mu_0\mu_l - \omega^2\varepsilon_0\mu_0\mu_l\right)^{1/2} \qquad (6)$$

and where t_l is the thickness, μ_l is the relative magnetic permeability, σ_l is the conductivity of the l th layer, and ε_0 is the dielectric permittivity of free space. In practice, the reciprocal of the conductivity, the resistivity ρ_l, is commonly used. Since we employ the quasi-static assumption, Eq. (6) becomes

$$k_l = \left(i\omega\sigma_l\mu_0\mu_l\right)^{1/2} \qquad (7)$$

In the half-space at the bottom of the electrical section,

$$Y_L = \hat{Y}_L \qquad (8)$$

Y_1 is a complex function of an integral variable λ, the angular frequency ω, the magnetic permeability μ, the resistivity ρ, and the thickness *t* of the layers. For a given model, Y_1 can be calculated using the recurrence relationship in Eqs. (3)-(5). Then, Y_1 can be substituted into Eq. (2) and then into (1) to yield the responses of the system over the model [17].

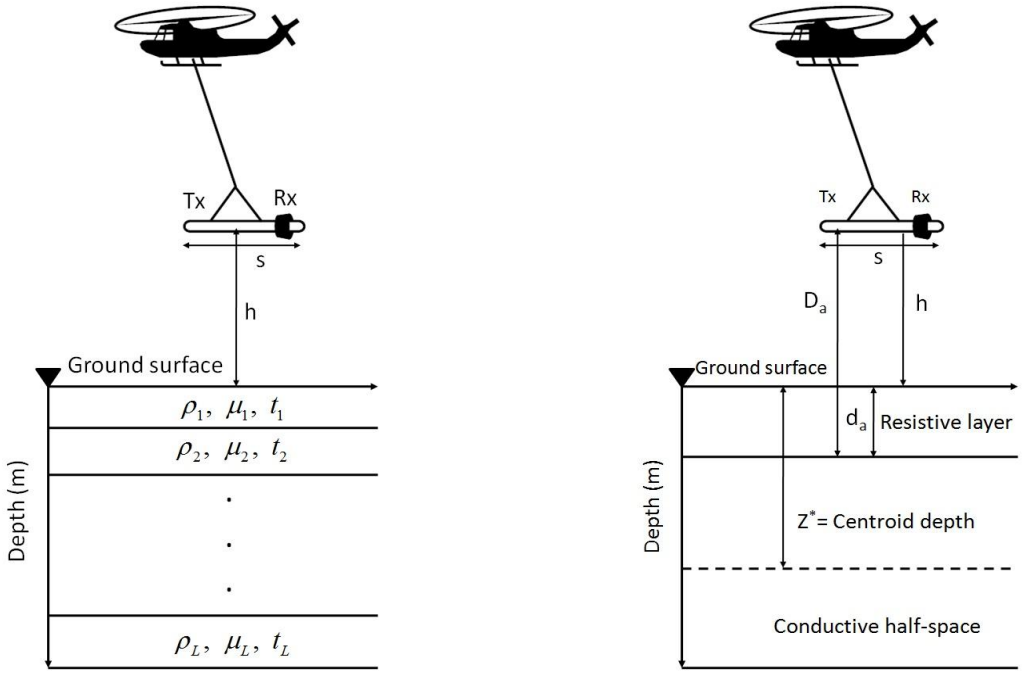

Figure 2. The geometry of the EM coplanar coil system over 1D earth models: a) the L-layer half-space, b) the homogenous half-space [reproduced from 27].

2.2 Approximate 1D inverse modeling of EM data

At each frequency, the two components of the secondary magnetic field, *R* and *Q*, and the sensor height *h* are measured. A resistivity-depth cross-section can be obtained if the apparent resistivity is displayed for each measured frequency *f* versus a specific depth, the centroid depth z^*(f) (Figure 2b). In summary, Mundry [4] used the following set of equations for each frequency *f* to plot a resistivity-depth cross-section,

$$\varepsilon = \frac{|Q|}{|R|} \tag{9}$$

$$z^*_{Mun} = \frac{1}{2} h\, \varepsilon^{1.23} \tag{10}$$

$$\rho_{Mun} = \frac{\omega \mu_0 h^2\, \varepsilon^{2.46}}{2} \tag{11}$$

where ε is the phase ratio. Here the resistivity ρ_{Mun} corresponds to the centroid depth z^*_{Mun} for the frequency *f*.

Over a homogeneous half-space earth model, the calculated sensor height or apparent distance, D_a shown in Figure 2b, equals to the measured sensor height *h*. For an inhomogeneous layered half-space, however, the apparent resistivity is an approximation to the true resistivity of the ground. In this case, the measured sensor height *h* is not necessarily equal to the calculated sensor height D_a. The difference between the calculated and the measured sensor height is called the apparent depth [3],

$$d_a = D_a - h \tag{12}$$

Considering the in-phase and quadrature components, amplitude ($A = \sqrt{R^2 + Q^2}$), and the phase ratio ε , the apparent resistivity and its corresponding depth are calculated by a set of curves shown in Figure 3 that illustrate logarithmic variation of transformed amplitude $A'^{1/3} = A^{1/3} / \gamma$ (where $\gamma = s / h$) or $\log(\varepsilon)$ versus $\log(\delta)$ (where $\delta = \frac{h}{p}$, and $p = \sqrt{\frac{2\rho}{\omega \mu_0}}$ is the skin depth). The apparent resistivity is obtained using the following relation,

$$\rho_{Sim} = \left(\frac{h}{\delta}\right)^2 \left(\frac{\omega \mu_0}{2}\right) \tag{13}$$

The apparent distance D_a is also calculated from the following relation,

$$D_a = s\left(A'/A\right)^{1/3} \quad (14)$$

A resistivity-depth image can be obtained from ρ_{Sim} and a modified centroid depth by Siemon 2001 [1] as follows,

$$Z^*_{Sim} = d_a + \frac{p}{2} \quad (15)$$

Figure 3 shows a 3-step way to acquire a resistivity-depth image using Siemon method [1]. The procedure of obtaining resistivity-depth data is as: (1) Calculating a phase ration from observed data at each frequency *f*, (2) Determining corresponded $\log(\delta)$ to obtain ρ_{Sim} and finally (3) finding the related amplitude in order to obtain D_a for calculating Z^*_{Sim}.

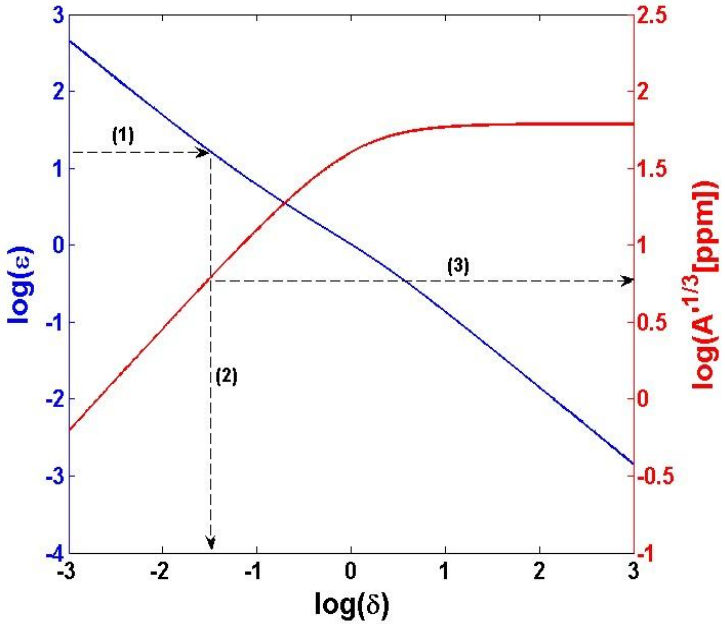

Figure 3. The curves present $\log(\varepsilon)$ and $\log(A'^{1/3})$ as a function of $\log(\delta)$, where $\delta = \frac{h}{p}$, *h* is the sensor height, and *p* is the skin depth (reproduced from [1]).

3. Application to synthetic data

Two synthetic 1D EM data which corrupted by 1% random Gaussian noise shown in Figure 4 are considered to evaluate the capability of the two aforementioned methods in order to plot a resistivity-depth sound of an earth model. The response of non-susceptible ($\mu_l = 1$) models were calculated in 15 frequencies within the range of 10 Hz to 256 KHz for a HC system with 8 m coil separation and a sensor height of 30 m. The forward Eq. (1) has been solved approximately by Guptasarma and Singh 1997 [32] digital linear filter for Hankel J_0 transform. The obtained result along depth applying both the Mundry and the Siemon methods are shown in Figure 4. Here, both embedded layers in comparison with the background resistivity are approximately recovered. As shown, the first layer in Figure 4a in comparison with the similar one of the second synthetic model in Figure 4b is conductive or has lower resistivity. When the first layers are conductive, the electrical current diffuses in the shallower layers so it may not easily penetrate in the deeper ones. Therefore, electrical imaging of deeper layers may be a problem in such cases in comparison with resistive overburden. This rule a bit affected recovering resistive embedded layer in Figure 4a.

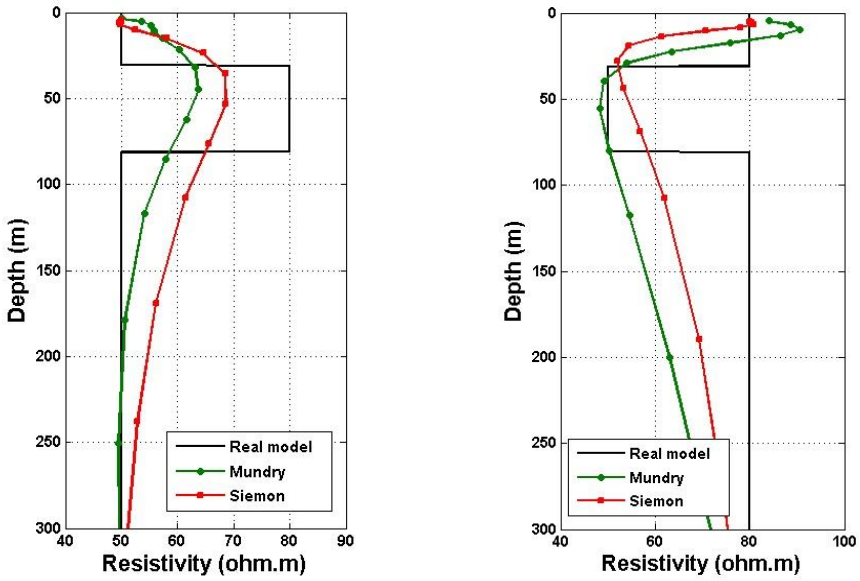

Figure 4. The results of synthetic 1D EM data inversion by the Mundry and the Siemon methods: a) a higher resistive embedded layer, and b) a lower resistive embedded layer in comparison with the background resistivity model.

In addition to 1D earth model, a 2D synthetic model shown in Figure 5b consisting of a four-layer model in which its upper layer contains a 2D conductive body of 50 Ohm.m with dimension of 100 m × 20 m is considered to apply the methods. Such a 2D model was also used in the many research works related to HEM data inversion [10, 20]. The third layer and the upper 2D body within the model are represented as a deep and shallow conductor, respectively, locating above a resistive basement of 1000 Ohm.m. The synthetic HEM data sets (response of non-susceptible 2D model) were calculated with a step size of 5 m using the improved Guptasarma and Singh 1997 forward code (Figure 5a). The computed components corrupted by 3% random Gaussian noise are for a five-frequency (387, 1820, 8225, 41550, and 133200 Hz) HC HEM system at a sensor altitude of h = 30 m and a coil separation of 8 m [10].

The approximate 1D inverse modeling was applied along the 2D synthetic model and then the constructed models were stitched together to give the 2D resistivity-depth images, displayed in Figures 5c and d for both methods. The recovered models approximately show smooth variation of resistivity in shallow depth while resistive basement could not be recovered properly. Using lower frequencies components can be useful to recover deeper variation in this case. Two direct inversion methods are partially able to detect the depth and the resistivity of the top layer (with resistivity of 200 Ohm.m) and also to locate the embedded 2D conductive body correctly. The boundary of high conductive layer at depth 50 m is not also sharp to be easily distinguished using such approximate methods.

Here, we have used approximate inversion methods for FEM data, i.e. the direct methods. Inverse modeling of such data needs more frequencies to obtain higher resolution models. Since we have a five-frequency dataset, for each data point along profile x, we acquire only five resistivity-depth points, so it does not produce a high resolution image along depth. The acquired results are completely related to the number of frequencies and the structure of the embedded layers at cross sections. The only way that we may improve the outputs is the application of iterative methods to retrieve a model with higher accuracy in inverse modeling. Since iterative methods consider multi-layered earth model under each observed data point, the resolution will increase by this assumption. Iterative methods in inverse modeling of frequency domain EM data are a bit time-consuming to be applying.

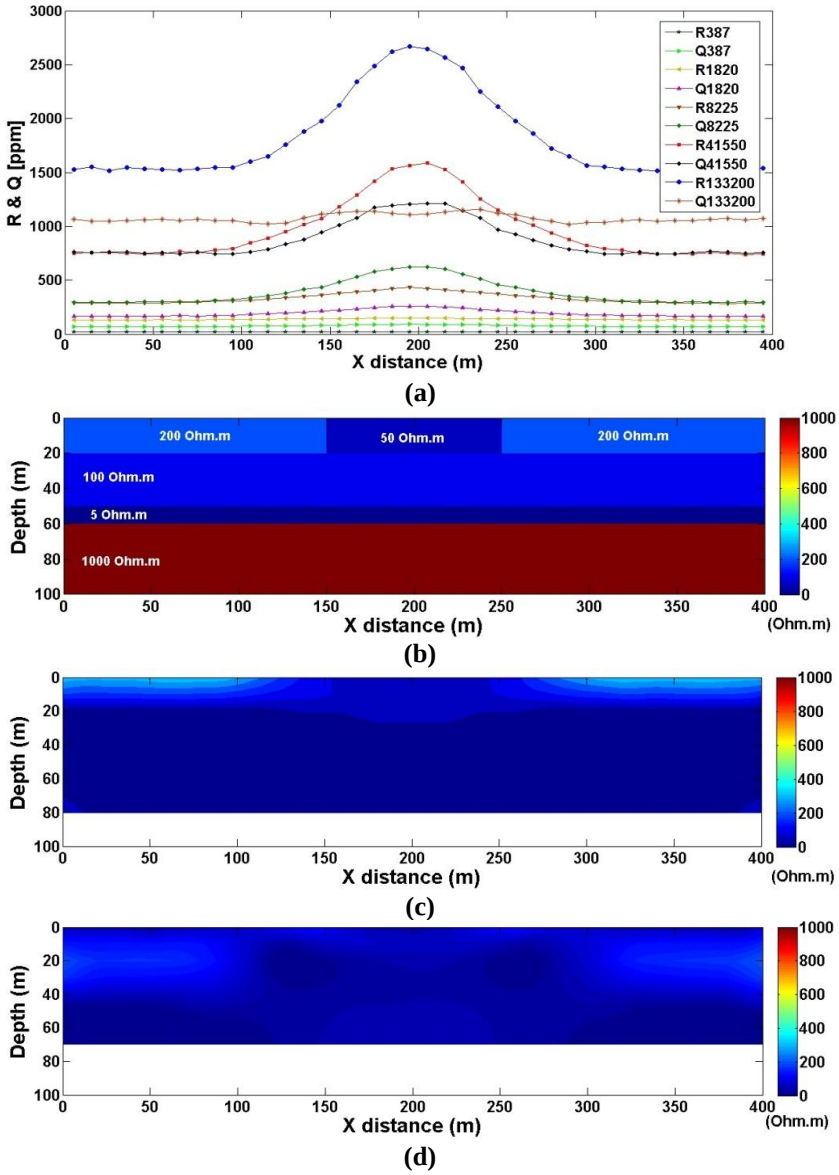

Figure 5. Inversion of a 2D EM cross-section along a 400 m profile: a) the observed components of five frequencies, b) Four-layer resistivity model containing a 2D conductive body of 50 Ohm.m in the top layer and a very conductive 10-m-layer at the depth of 50 m, c) the result of the Mundry method, d) the result of the Siemon method.

4. Background geology

The study area called Kalat-e-Reshm is located in Semnan province to the east of Tehran, capital city of Iran (Figure 6). The main purpose of this prospect is to explore new sulphide mineralization, especially porphyry copper. There are two porphyry copper deposits, which are located to the west and the northeast of the conducted airborne survey over the area. The oldest rocks in the area include the Precambrian metamorphic rocks with outcrops in the eastern part of the area and are composed of gneiss, amphibolites, and mica-schist. The geological studies in the area reveal that the volcanic rocks are mainly andesite, basalt, ryolite and dacite that contain layers of sandstone, siltstone and conglomerates.

There is an arc like outcrop in the survey area which is composed of andesitic porphyry. Erosion has ruined some parts of this arc and some other parts are covered by alluvium. Right at the north of the arc there is another feature including green to buff marl, conglomerate, sandstone, shale and tuff. Both structures belong to Tertiary. In the northeast of the

area, an alluvium channel including tuff, sandstone, conglomerate, schist, mica-schist, andesitic–basaltic lava, ultrabasic rocks and marble crosses metavolcanic structures of Paleozoic period. All these alluviums accumulate as high level piedmont and alluvial fans over the arc and continue to the south of the arc. The dominant part of the area is covered by a mixture including sandstone, tuff, conglomerate, andesitic and volcanic rocks as well as shale and marl. Here we work on a trapezoid-shaped area shown on the geological map with dash line, which has been covered by an airborne magnetic and FEM survey under supervision of the Geological Survey of Iran (GSI) [22].

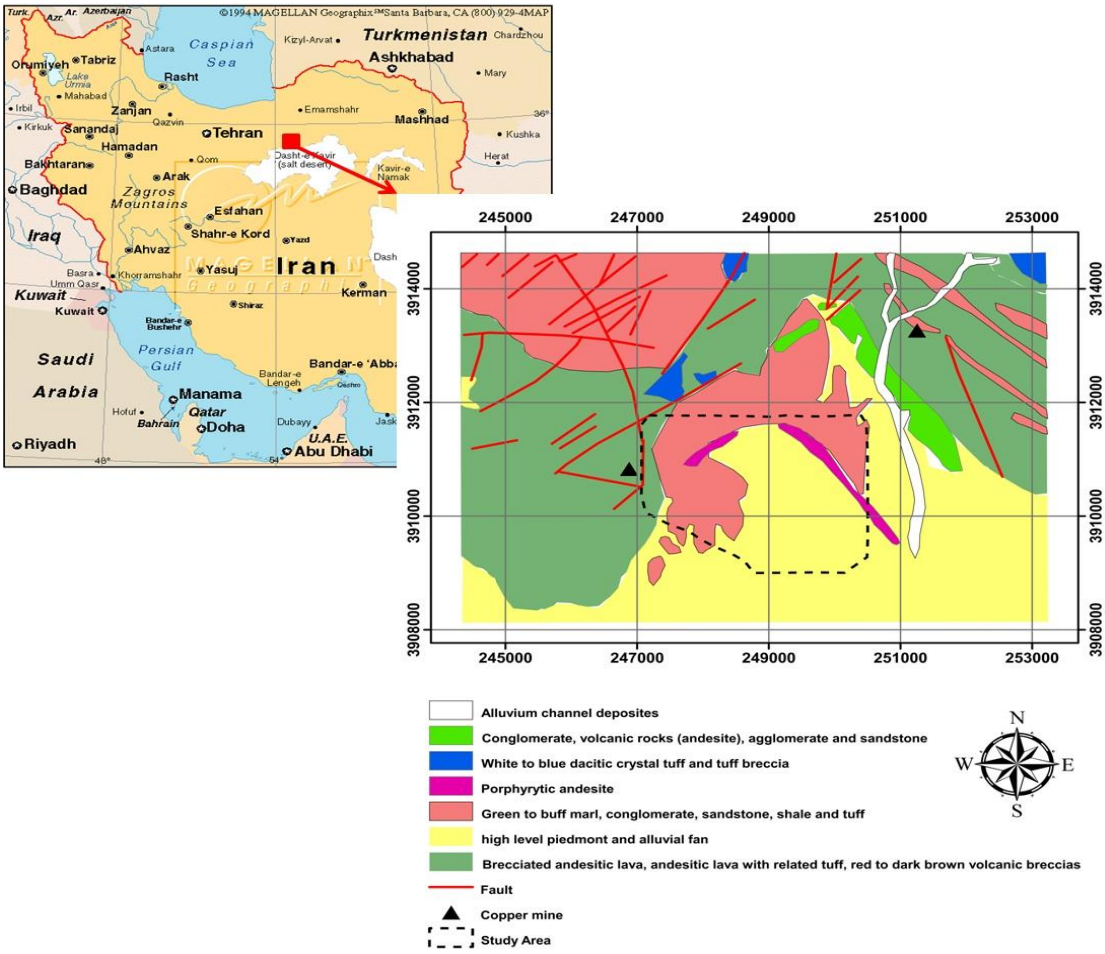

Figure 6. The Geology map of the Kalat-e-Reshm area with location of the study area (reproduced from [22]).

5. Real data inversion

The Geological Survey of Iran (GSI) conducted an airborne survey over the Kalat-e-Reshm area in 2003 (Figure 7). The line spacing is 200 m and the flight height varies between 30 and 60 m. The data acquisition sampling distance along flight lines is nearly 4 m. GSI uses a DIGHEM data acquisition system for the HEM measurement with a bird that measured HC configurations components for three frequencies including 875, 4920 and 33,000 Hz. The distance between all the coil pairs is 6.4 m. For the sake of inversion, data were sample at every six stations meaning that the sampling interval is approximately 24 m. The total magnetic field data are also measured using a caesium magnetometer which is attached to the bird. The observed FEM components along flight lines for tree frequencies are shown in Figure 8. The low frequency components of 875 Hz, which scans deeper levels of the ground surface, significantly located the trace of this geological unit (Figures 8a and 8b). Indeed, it confirms the occurrence of the desired geological unit at depth.

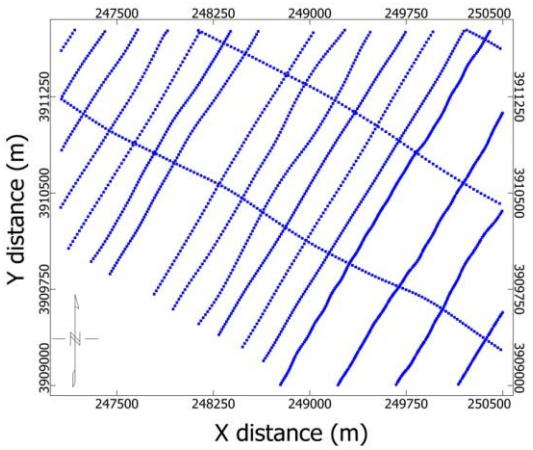

Figure 7. Geophysical survey lines over the study area, simultaneously measuring magnetic and FEM data.

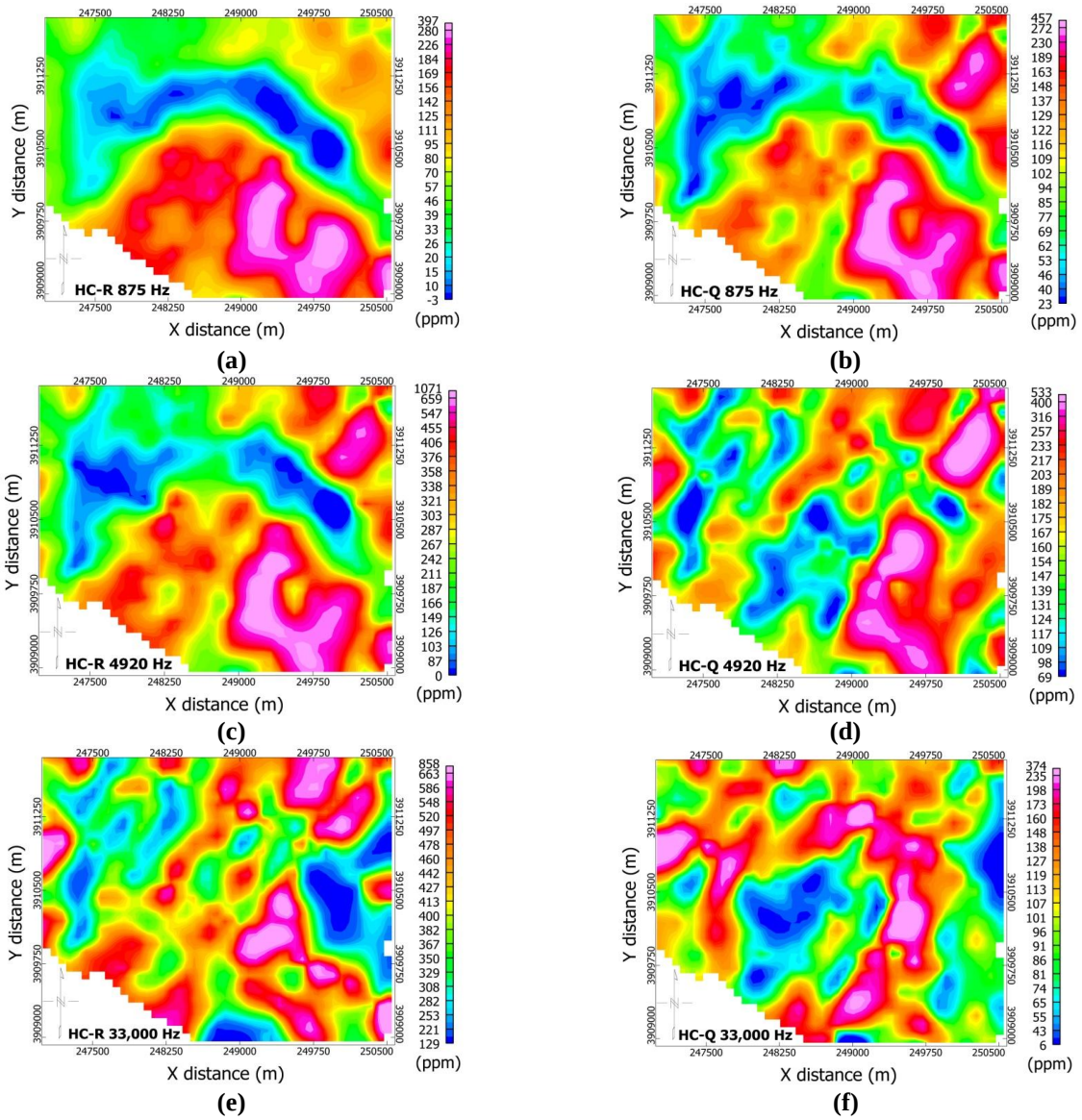

Figure 8. The real (R) and quadrature (Q) components of the observed horizontal coplanar (HC) data for three frequencies including: a) R-875 Hz, b) Q-875 Hz, c) R-4920 Hz, d) Q-4920 Hz, e) R-33 KHz, and f) Q-33 KHz.

Applying two approximate 1D direct inversion methods generates similar resistive geological structure in accordance with the desired arc-shaped porphyry andesite shown on the geological map. The two recovered models from 1D inverse modeling of FEM data visualized in 3D are shown in Figure 9. Based on the geological map shown in Figure 6, the andesite unit is embedded in the high level piedmont and alluvial fan as well in a background with shale, sandstone and tuff. Since this background consists of some sedimentary units, it causes a conductive background in comparison with the resistive andesite unit which is the aim of prospect. The recovered models show that the porphyry andesite extends down at depth and may have potential of mineral occurrences related to porphyry type sources. This geologically plausible model of the porphyry andesite needs to be drilled by some exploratory boreholes to evaluate its capability for mineral occurrences.

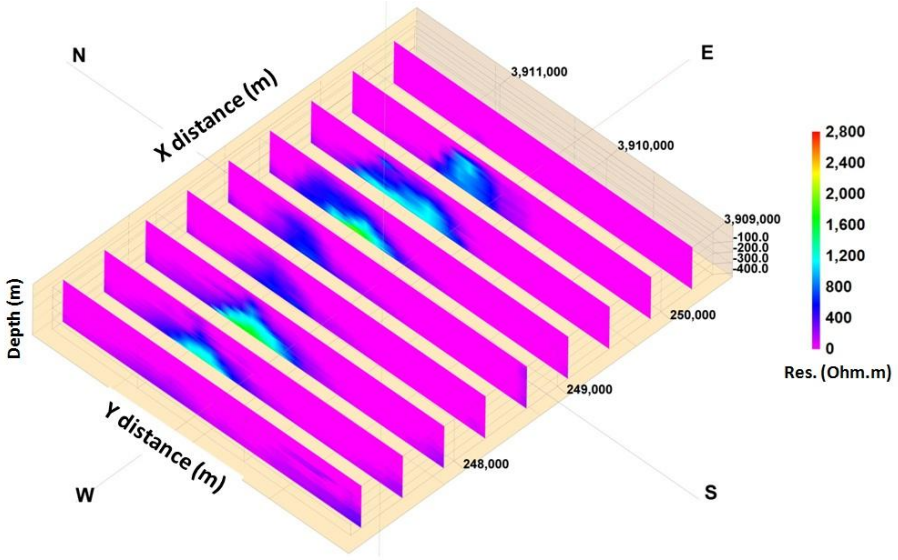

(a)

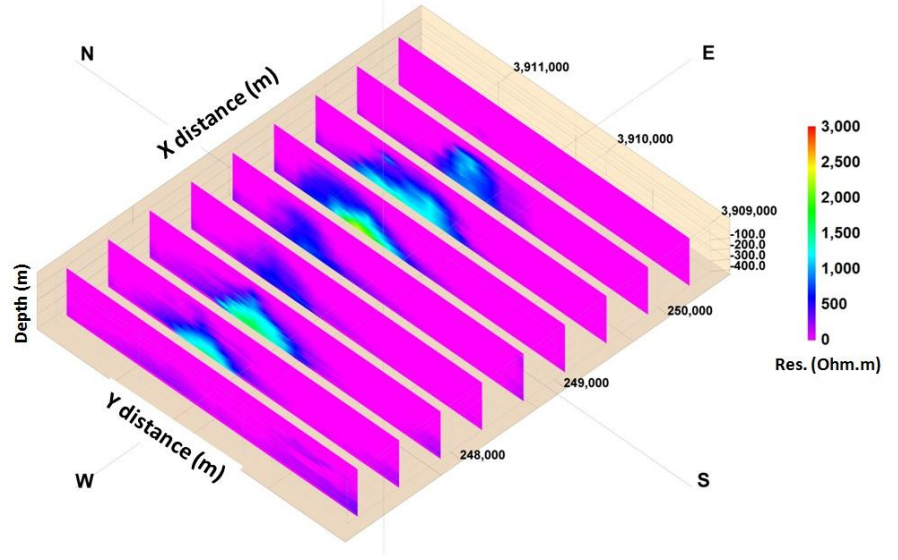

(b)

Figure 9. 3D visualization of 1D approximate inversion of HC data: a) the Mundry model, b) the Siemon model. Both recovered models prove the existence of a resistive unit which corresponds to the arc-shaped porphyry andesite shown on the geological map in Figure 6.

The HEM data are sensitive to the magnetic susceptibility of the probable buried sources which cause negative-in-phase values, especially at low frequencies [14, 18]. In this study, as obvious from observed data shown in Figure 8, we are working on a low susceptible background since positive observations exist except some negative ones. Therefore, the background susceptibility of the study area has trivial effect on the recovered resistivity models. The residual reduced-to-pole (RTP) map of the observed magnetic data in the study area is shown in Figure 10 while the location of the arc-shaped porphyry andesite has been conspicuously enhanced. At the time of airborne survey, the magnetic declination and inclination were $3^{\circ}38$ and $53^{\circ}28$ respectively.

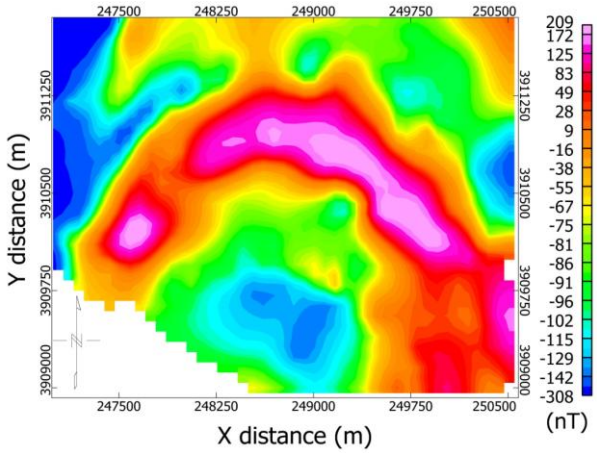

Figure 10. The residual RTP map of the observed magnetic data at the Kalat-e-Reshm area which enhances the location of arc-shaped porphyry andesite shown on the geological map in Figure 6.

Inversion of large scale magnetic data needs tackling two problems; (a) fast forward modelling and (b) using an efficient and fast solver for central system of equations like the conjugate gradient (CG) method. In the cases of using several hundred thousand model parameters and tens of thousands of data, the main problem of inversion is related to fast computation of the forward operator. For such problems, especially airborne potential survey, a compression technique like sparsity based representation of the forward operator by wavelet transforms can be used. After solving the problem of the forward mapping, a fast solver like the CG method can be applied to compute model parameters [23, 33 & 34]. In this study, we have used a fast approximate magnetic inversion method called the Lanczos bidiagonalization approach, which has been previously developed to work as a fast solver for central system of equations in magnetic inversion [23]. Our motivation is fast recovery of 3D magnetic susceptibility distributions. To do this, an iterative method is applied. Where, the original system of equations is replaced by a system of lower dimension to increase the speed of the solution procedure significantly while being able to solve the original problem with a high degree of accuracy.

To perform an approximate 3D magnetic inversion method, the study area is divided into 43×40×20= 34,400 rectangular prisms with dimension 80×70×20 m in *x*, *y* and *z* directions respectively. The Lanczos method considering 20 steps has been applied to recover a 3D susceptibility model shown in Figure 11. Interested readers are referred to the paper published by Abedi et al. 2013 to learn how the method can be applied in detail. The magnetic susceptibility model shows location of an arc-shaped porphyry andesite unit which also corresponds to the real location of the resistive models by the Mundry and the Simone approximate methods. Most of the recovered susceptibility values are lower than 0.03 (in SI unit) that shows a low susceptible porphyry unit. For this reason, most of the observed in-phase data points of the HC system are positive. Certainly higher susceptibility sources cause negative values of in-phase components.

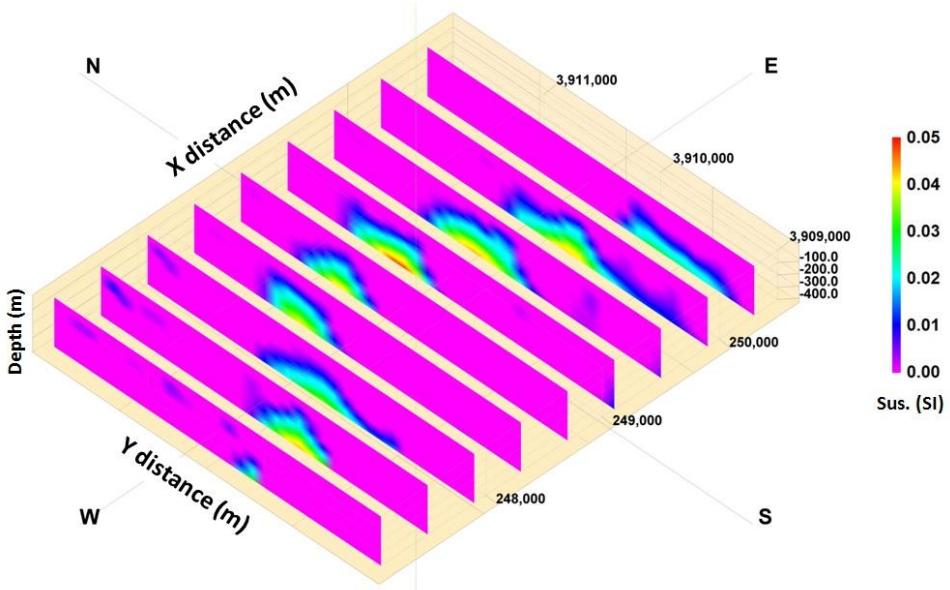

Figure 11. 3D view of magnetic inversion result at the Kalat-e-Reshm area considering 20 steps of the Lanczos bidiagonalization method. The recovered model proves the existence of a low susceptible unit which corresponds to the arc-shaped porphyry andesite shown on the geological map in Figure 6.

The susceptible-resistive porphyry andesite model constructed based on the approximate methods shows a thicker structure than what is shown on the geological map in Figure 6 while it extends down at depth. Because of the evidences, i.e., two sources adjacent to this unit, drilling in such structure can be promising to evaluate the capability of this source for mineral occurrences, especially porphyry copper.

6. Conclusions

In this study we have used an integrated geophysical method based on simultaneously modeling of airborne electromagnetic and magnetic data in order to image the extension of a geological porphyry unit with higher certainty at depth that have potential of mineral occurrences in the Kalat-e-Reshm area, Semnan province of Iran. Recovered resistivity model of the porphyry andesite from 1D approximate inversion of the frequency domain electromagnetic data showed a resistive structure for both the Mundry and the Simone methods. This geological structure has been embedded in a conductive background consisting of sedimentary units. In order to reduce the uncertainty arising from single geophysical dataset interpretation, the 3D inversion of magnetic data in the study area by the Lanczos bidiagonalization as a fast approach in the inverse modeling of geophysical potential data was also implemented. The constructed magnetic susceptibility model revealed a low susceptible porphyry unit which was in accordance with the location of resistive model retrieved from airborne electromagnetic data. The output of this integrated study confirmed a susceptible-resistive porphyry unit while going down at depth. This structure may have high potential of mineral occurrences, especially porphyry copper due to adjacent to some previously working mines in the study area.

Acknowledgements

The authors gratefully acknowledge the support provided by the faculty of Mining Engineering, University of Tehran. We thank the Geological Survey of Iran (GSI) for data preparation. We would like to express sincere thanks to Dr. Farzad Shirzaditabar at Razi University, Kermanshah, Iran for helping us to access the data. The work presented here was funded by Tehran DaneshKan Technical Institute (TDTI).

References

[1]. Siemon, B. (2001). Improved and new resistivity-depth profiles for helicopter electromagnetic data. Journal of Applied Geophysics, 46: 65–76.

[2]. Siemon, B. (1997). Verbesserte Algorithmen zur Bestimmung von Sondierungskurven in der Hubschrauber elektromagnetik. Bundesanstalt fu¨r

Geowissenschaften und Rohstoffe, Report No. 115920, Hannover (unpublished), 81 pp.

[3]. Fraser, D.C. (1978). Resistivity mapping with an airborne multicoil electromagnetic system. Geophysics, 43: 144–172.

[4]. Mundry, E. (1984). On the interpretation of airborne electromagnetic data for the two-layer case. Geophysical Prospecting, 32: 336-346.

[5]. Huang, H. and Fraser, D.C. (1996). The differential parameter method for multifrequency airborne resistivity mapping. Geophysics, 61: 100-109.

[6]. Sengpiel, K.P. (1988). Approximate inversion of airborne EM data from a multi-layered ground. Geophysical Prospecting, 36: 446– 459.

[7]. Sengpiel, K.P. (1990). Theoretical and practical aspects of ground-water exploration using airborne electromagnetic techniques. In: Fitterman, D. V. (ed.), Proceedings of the USGS Workshop on Developments and Applications of Modern Airborne Electromagnetic Surveys, 1987, Golden, Colo., USGS Bulletin 1925, 149-154.

[8]. Arabamiri, A.R., Moradzadeh, A., Rajabi, D., Fathianpour, N. and Siemon, B. (2010). Investigation of forward modeling accuracy in HEM data inverse modeling. Geosciences Scientific Quarterly Journal, 20: 137-140 (Published in Persian).

[9]. Arabamiri, A.R., Moradzadeh, A., Rajabi, D., Siemon, B. and Fathianpour, N. (2010). Definition and comparison of improved Mundry's integral on HEM data inverse modeling. Geosciences Scientific Quarterly Journal, 19: 115-118 (Published in Persian).

[10]. ArabAmiri, A.R., Moradzadeh, A., Fathianpour, N., and Siemon, B. (2010). Inverse modeling of HEM data using a new inversion algorithm. Journal of Mining & Environment, 1: 9-20.

[11]. Fullagar, P.K. and Oldenburg, D.W. (1984). Inversion of horizontal loop electromagnetic frequency sounding. Geophysics, 49: 150–164.

[12]. Farquharson, C.G. and Oldenburg, D.W. (1993). Inversion of time-domain electromagnetic data for a horizontally layered earth. Geophysical Journal International, 114: 433–442.

[13]. Fitterman, D.V. and Deszcz-pan, M. (1998). Helicopter EM mapping of saltwater intrusion in Everglades National Park, Florida. Exploration Geophysics, 29: 240–243.

[14]. Zhang, Z. and Oldenburg, D.W. (1999). Simultaneous reconstruction of 1-D susceptibility and conductivity from electromagnetic data. Geophysics, 64: 33-47.

[15]. Zhang, Z., Routh, P.S., Oldenburg, D.W., Alumbaugh, D.L. and Newman, G.A. (2000). Reconstruction of 1-D conductivity fromdual-loop EM data. Geophysics, 65: 492–501.

[16]. Sengpiel, K.P. and Siemon, B. (2000). Advanced inversion methods for airborne electromagnetic exploration. Geophysics, 65: 1983– 1992.

[17]. Huang, H. and Fraser, D.C. (2003). Inversion of helicopter electromagnetic data to a magnetic conductive layered earth. Geophysics, 68: 1211–1223.

[18]. Farquharson, C.G., Oldenburg, D.W. and Routh, P.S. (2003). Simultaneous 1D inversion of loop- loop electromagnetic data for magnetic susceptibility and electrical conductivity. Geophysics, 68: 1857–1869.

[19]. Farquharson, C.G. and Oldenburg, D.W. (2004). A comparison of automatic techniques for estimating the regularization parameter in non-linear inverse problems. Geophysical Journal International, 156: 411-425.

[20]. Siemon, B., Auken, E. and Christiansen, A.V. (2009). Laterally constrained inversion of helicopter-borne frequency-domain electromagnetic data. Journal of Applied Geophysics, 67: 259–268.

[21]. Dao-Qing, Z., Lin, T., Han-Dong, T., Hong-Rui, Z., Xue, Y. and Wei-Ping, W. (2010). Inversion of frequency domain helicopter-borne electromagnetic data with Marquardt's method. Chinese Journal of Geophysics, 53: 189-197.

[22]. Shirzaditabar, F., Bastani, M. and Oskooi, B. (2011). Imaging a 3D geological structure from HEM, airborne magnetic and ground ERT data in Kalat-e-Reshm area, Iran. Journal of Applied Geophysics, 75: 513-522.

[23]. Abedi, M., Gholami, A., Norouzi, G.H. and Fathianpour, N. (2013). Fast inversion of magnetic data using Lanczos bidiagonalization method. Journal of Applied Geophysics, 90: 126-137

[24]. Shirzaditabar, F. and Oskooi, B. (2010). Recovering 1D conductivity from AEM data using Occam inversion. Journal of the Earth and Space Physics, 37: 47-58.

[25]. Shirzaditabar, F. and Oskooi, B. (2011). Approximate interpretation of Airborne Electromagnetic data using a half-space model. Journal of the Earth and Space Physics, 38: 1-12.

[26]. Shirzaditabar, F., Bastani, M. and Oskooi, B. (2011). Study of the effects of the variables changes on the inversion of airborne electromagnetic data in frequency domain. Iranian Journal of Geophysics, 5: 38-50.

[27]. Kirsch, R. (2009). Groundwater Geophysics, A tool for Hydrogeology. 2nd, 548 p., Springer.

[28]. Siemon, B., Christiansen, A.V. and Auken, E. (2009). A review of helicopter-borne electromagnetic methods for groundwater exploration. Near Surface Geophysics 7, 629-646

[29]. Frischknecht, F.C. (1967). Fields about an oscillating magnetic dipole over a two-layer earth and application to ground and airborne electromagnetic surveys: Quarterly of the Colorado School of Mines 62, No.1.

[30]. Ward, S.H. (1967). Electromagnetic theory for geophysical applications, in Ward, S.H., Ed., Mining Geophysics 2, Theory: Soc. Expl. Geophys., 13-196.

[31]. Ward, S.H. and Hohmann, G.W. (1997). Electromagnetic theory for geophysical applications, *in* Nabighian, M.N., Ed., Electromagnetic methods in applied geophysics, 1, Theory: Soc. Exp. Geophys., 130-311.

[32]. Guptasarma, D. and Singh, B. (1997). New digital linear filters for Hankel J_0 and J_1 transforms. Geophysical Prospecting, 45: 745-762.

[33]. Li, Y. and Oldenburg, D.W. (2003), Fast inversion of large-scale magnetic data using wavelet transforms and a logarithmic barrier method. Geophys. J. Int. 152, 251-265.

[34]. Namaki, L., Gholami, A. and Hafizi, M.A. (2011). Edge-preserved 2-D inversion of magnetic data: an application to the Makran arc-trench complex. Geophys. J. Int. 184, 1058-1068.